J. Fluid Mech. (1965), *vol.* 23, *part* 1, *pp.* 77–98
Printed in Great Britain

Laminar free convection in a vertical slot

By J. W. ELDER
Department of Applied Mathematics and Theoretical Physics, Cambridge†

(Received 6 November 1964 and in revised form 10 May 1965)

This is largely an experimental study of the interaction of buoyancy and shear forces in the free convective flow of a liquid in a rectangular cavity across which there is a uniform temperature difference, ΔT, produced by maintaining the two vertical walls at two different temperatures. The height of the cavity, H, is made larger than the width of the cavity, L, and the cavity is sufficiently long in the third dimension for the mean flow to be nearly everywhere two-dimensional. The flow is specified by three dimensionless parameters: σ, the Prandtl number; $h = H/L$, the aspect ratio; $A = \gamma g \Delta T L^3/\kappa\nu$, the Rayleigh number. The experiments are generally restricted to $h = 1$–60, $\sigma \doteqdot 10^3$ and $A < 10^8$.

For $A < 10^3$ the temperature field closely satisfies Laplace's equation but a weak stable unicellular circulation is generated. The flow is vertical throughout the slot except for regions within a distance of order L from the ends.

For $10^3 < A < 10^5$, large temperature gradients grow near the walls, and in an interior region a uniform vertical temperature gradient is established. The flow is similar to that near an isolated, heated, vertical plate except that the vertical growth of the wall layers is inhibited in the central part of the slot by the presence of the other layer which prevents entrainment of fluid.

Near $A = 10^5$ the interior region of the flow generates a steady secondary flow. A regular cellular pattern becomes superimposed on the basic flow to produce a 'cats-eye' pattern of streamlines. Near $A = 10^6$ when the secondary cell amplitude is large, a further steady cellular motion is generated in the weak shear regions between each cell.

1. Preliminary remarks

Many geophysical and astrophysical phenomena are maintained by buoyancy forces, but the role of these forces is generally strongly modified by co-existing shear, rotation of the system as a whole, processes at a free surface, and so on. The free convection of a viscous fluid in a vertical slot, whose walls are held at two different temperatures, provides one of the simplest cases of an interaction between buoyancy and shearing forces; a study of this interaction is the central theme of this paper.

This investigation was started simply as an attempt to obtain an experimental visualization of the boundary-layer flows which precede and follow the onset of

† Present address: Institute of Geophysics and Planetary Physics, University of California, La Jolla, California.

convective turbulence, but it was soon discovered that the primary laminar circulatory flow does not at first produce boundary-layer waves but, rather, steady large-scale secondary flows appear in the interior of the slot. Further, it was found that these secondary flows, when of sufficient amplitude, were able to generate other steady secondary flows, to be called tertiary flows. Here we discuss the primary circulatory flow and the steady secondary flows which can grow in it, leaving for another paper the study of the unsteady disturbances and the subsequent turbulent flow.

2. Statement of the problem

2.1. *Dimensional analysis*

Consider the arrangement shown in figure 1. A hollow rectangular prism of width L, breadth B and height H has a co-ordinate frame $OXYZ$ with its origin located in one corner. The face $x = L$ is maintained at temperature T_0, the face

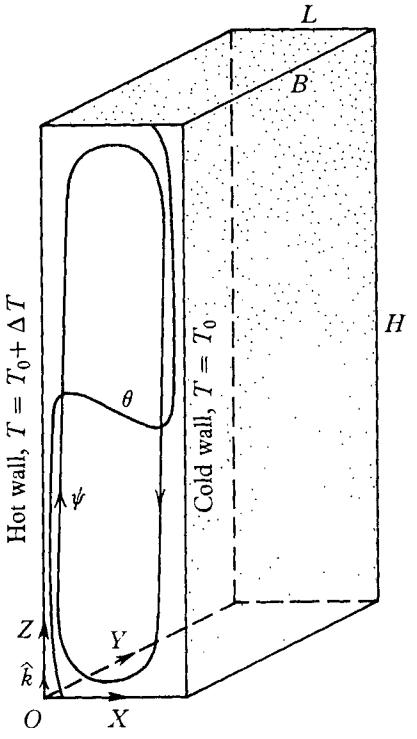

FIGURE 1. Diagram of the slot. (Note: in all diagrams the hot wall is on the left-hand side.)

$x = 0$ at temperature $(T_0 + \Delta T)$ and the other walls are insulated. Provided B is sufficiently greater than L, the primary motion of the fluid which fills the prism will be nearly everywhere two-dimensional and confined to planes $y = \text{const.}$, except near $y = 0$, B. In the analysis $B/L = \infty$. A possible isotherm and streamline is shown projected on $y = 0$ in figure 1.

Making the Boussinesq approximation, that density variations are significant only in their generation of buoyancy forces, and that other fluid parameters are independent of temperature, the problem is defined by: the kinematic viscosity, ν;

the thermal diffusivity, κ; the acceleration due to buoyancy, $\gamma g \Delta T$, where γ is the coefficient of cubical expansion; L and H. Hence, since these involve only the dimensions of length and time, three dimensionless parameters are needed to specify the system. A convenient set is:

$$S^2 \equiv \sigma = \nu/\kappa, \quad \text{Prandtl number;} \tag{1a}$$

$$A = \gamma g \Delta T L^3/\kappa\nu, \quad \text{Rayleigh number;} \tag{1b}$$

$$h = H/L, \quad \text{aspect ratio.} \tag{1c}$$

The field variables can be conveniently made dimensionless by choosing *units* of length, temperature, pressure, velocity:

$$L, \quad \Delta T, \quad \rho_0 Lg, \quad (\kappa\nu)^{\frac{1}{2}}/L. \tag{2}$$

Where confusion may arise, dimensional variables are written with an asterisk (*). The dimensionless temperature is written as θ. We shall write $\bar{x} = 1 - x$.

2.2. *Other investigations*

Batchelor (1954) has given a theoretical analysis of the problem, the case $A < 10^3$ being treated in some detail, but for large A only a qualitative discussion is possible. Batchelor's work, like that of Pillow (1952), suggests that as $A \to \infty$ the inner region has both constant non-zero vorticity and constant temperature. Eckert & Carlson (1961) have obtained with an interferometer, detailed observations of the primary temperature distribution in air ($\sigma = 0{\cdot}7$) and, in particular, measurements of the local heat transfer at the walls. They substantially confirm Batchelor's calculations at small A, but at large values of A find no evidence for Batchelor and Pillow's contention that the inner region will have a constant temperature; rather, they find a region of constant vertical temperature-gradient. These observations are confirmed by Mordchelles-Regnier & Kaplan (1963) using carbon dioxide gas at high pressures. Further evidence that the inner region has a constant vertical temperature-gradient and also zero vorticity is given in a calculation by Weinbaum (1964) and some experiments by Martini & Churchill (1960) for convection in a horizontal cylinder.

2.3. *The present investigation*

The experiments reported here are generally restricted to $h = 1$–60, $\sigma \doteqdot 10^3$ and $A < 10^8$. Near $A = 10^7$ the wall region becomes unstable; travelling wave systems grow independently on both the hot and cold walls. At $A = 10^9$, the central portion of the slot is turbulent. The flows for $A > 10^8$ will be discussed in another paper.

Our interest will centre around: (i) the uniform vertical temperature gradient β found in the interior of the flow for $A > 10^4$; and (ii) the mechanics of the secondary flows. It is found for $A > 10^5$, that $\beta h = \text{const.}$, independent of S and A. In this case the flow in the central portion of the slot is most strongly influenced by $m \equiv (\frac{1}{4}\beta A)^{\frac{1}{4}}$. Secondary flows appear for $m \geqslant 2\pi$.

The experimental observations are discussed in § 3–5, followed by an analytical discussion in § 6–8.

3. Experimental method

The flows were established in a rectangular cavity, two walls of which were maintained at two constant but different temperatures by pumping water from two thermostatic units through cavities behind the walls. The temperature difference ΔT was held constant to generally better than $\pm 0{\cdot}05\,^{\circ}\mathrm{C}$, the metal walls ensuring a negligible vertical temperature-gradient in the walls (measured values, no more than $0{\cdot}01/H$, °C/cm). The lower end of the cavity was packed with an insulator, either a block of porous rubber or Perspex; the upper (free) surface of the fluid was left undisturbed in contact with a dead-air space above the filled portion of the cavity. Thus, the boundary conditions on the upper fluid surface differ from those on the lower surface, but this was the most convenient arrangement for probe access.

Velocity measurements were made by direct observation through the glass or Perspex sides ($y^* = 0, B$) of aluminium powder suspended in the fluid; either visually, by timing the passage of a single particle between fixed marks in the eyepiece of a travelling microscope, or from time photographs, in which the streak-length is proportional to the velocity. Where possible, the plane of observation was chosen halfway between the glass sides. Velocities are accurate to better than $\pm 5\,\%$. A very helpful point is that aluminium particles are roughly disk-shaped and tend to lie with the plane of the disk on the stream surface, so that the broad features of the stream surfaces are immediately apparent.

Temperatures were measured with copper-constantin thermocouples and a potentiometer to $\pm 0{\cdot}01\,^{\circ}\mathrm{C}$. A probe was entered from above; the lower end was of diameter 1 mm, with 3 cm of the thermocouple wires (46 S.W.G.) sticking out of the end. Direct observation showed very little disturbance to the flow due to the presence of the probe, except for a very slow drift of the cellular pattern.

Three experimental arrangements were used:

Apparatus I: $H \leqslant 60$ cm; $B = 5$ cm; $L = 1, 2, 3, 4, 5$ cm.

Apparatus II: $H \leqslant 80$ cm; $B = 10$ cm; $L = 4{\cdot}08$ cm.

Apparatus III: $H = 55$ cm; annular cylinder of radii 3·3 cm, 6·3 cm; $L = 3$ cm.

The initial study was with apparatus III, in which the discovery of the vertical temperature-gradient and the cats-eye mode were first made. This apparatus was supplied with a uniform heat flux on the inner boundary wall.

Apparatus I was designed so that L could be set to an arbitrary value, while apparatus II was specifically designed for the turbulence work.

Two fluids were used: medicinal paraffin and a silicone oil MS 200/100 centistoke. They both allow studies over the Rayleigh-number range of the experiments using apparatuses of convenient size and temperature differences sufficiently large for accurate measurement. A particularly convenient feature is the ease with which aluminium powder can be suspended. Such viscous oils necessarily have high Prandtl numbers so that in effect the 3 parameters (1) are reduced to 2. Both oils have similar properties, but paraffin has a very much larger variation of viscosity with temperature. The specification (1) requires γ, κ, ν to be independent of temperature and $\gamma \Delta T \ll 1$. Within the present experimental accuracy these requirements are satisfied except that the variation of viscosity with temperature

is large. In the specification (1) ν is evaluated (somewhat arbitrarily) at $(T_0 + \frac{1}{2}\Delta T)$. At larger values of ΔT the lower local viscosity near the hot wall produces noticeable asymmetry in the flow—e.g. the velocity profile is thinner and the velocity amplitude greater at the hot wall.

A further departure from ideal behaviour is the existence of three-dimensional effects due to finite values of L/B. Even for $L/B = 1$, at sufficiently high values of A, the motion is closely two-dimensional. The relevant parameter is δ^*/B, where δ^* is the wall-layer thickness, and, provided this is small, three-dimensional effects will be small. Nevertheless, there can be no motion on the faces $y = 0, B$, so that it is necessary to make observations well away from the faces. This raises a difficulty with the photographic technique for measuring the velocities, because particles moving near $y = 0, B$ tend to obscure the interior flow.

The reader should keep in mind the asymmetry produced by viscosity variations and three-dimensional effects produced by the side walls when inspecting the visualization photographs.

4. Experimental data for the primary flow

4.1. *Temperature distribution*

The temperature distribution has already been studied in some detail by Eckert & Carlson (1961); they have used their data to evaluate the local Nusselt number as a function of position on the slot wall, and in particular include a study of the low-Rayleigh-number case. For $A < 10^3$ the temperature field nearly everywhere closely satisfies Laplace's equation, so that $\theta \doteqdot (1-x)$, for which the heat flux is conductive and horizontal. There is no vertical temperature-gradient. The temperature field is such that the fluid is not in hydrostatic equilibrium; clearly a column of fluid near the cold wall has greater weight than a similar column near the hot wall, and a weak, steady circulation of constant sign is generated in the slot. This is a uni-cellular motion with fluid ascending in $0 < x < \frac{1}{2}$, descending in $\frac{1}{2} < x < 1$, buoyancy forces balancing viscous forces. The heat transported by the flow is negligible except for small contributions near the ends. As A increases, the temperature progressively departs from $\theta \doteqdot (1-x)$, the isotherms becoming S-shaped, as sketched in figure 1. The changes in the temperature field are initially most marked near the bottom of the hot wall and the top of the cold wall.

Here, our interest is directed toward understanding the primary flow in the case of strong convection, particularly insofar as it produces the secondary flows. Figure 2, therefore, shows the temperature distribution in a slot with $h = 20$, $A = 4{\cdot}0 \times 10^5$, when the primary flow is approaching the condition under which the secondary flow appears.

Three regions can be distinguished: a *wall* region, an interior region, and an *end* region. In the wall region $0 < (x, \bar{x}) < 0{\cdot}2$, the isotherms are slightly inclined to the wall with the temperature gradient being nearly horizontal—the temperature gradients are largest here. The interior region $0{\cdot}2 < x < 0{\cdot}8$ has nearly horizontal, regularly spaced isotherms from $\theta = 0{\cdot}35$ to $0{\cdot}65$, a region of nearly uniform, positive, vertical temperature gradient. Near the ends $z < 0{\cdot}1h$, $> 0{\cdot}9h$ the pattern is strongly influenced by the end boundary conditions.

The end regions can be regarded as buffers between the end boundary conditions and the nearly unidirectional flow between them. Here both ends are regions of outward heat flow. This differs from Eckert & Carlson's experiments, where θ_z is everywhere positive; they have insulators at both ends but here the upper end is a free surface which loses heat to the air space above. The end region

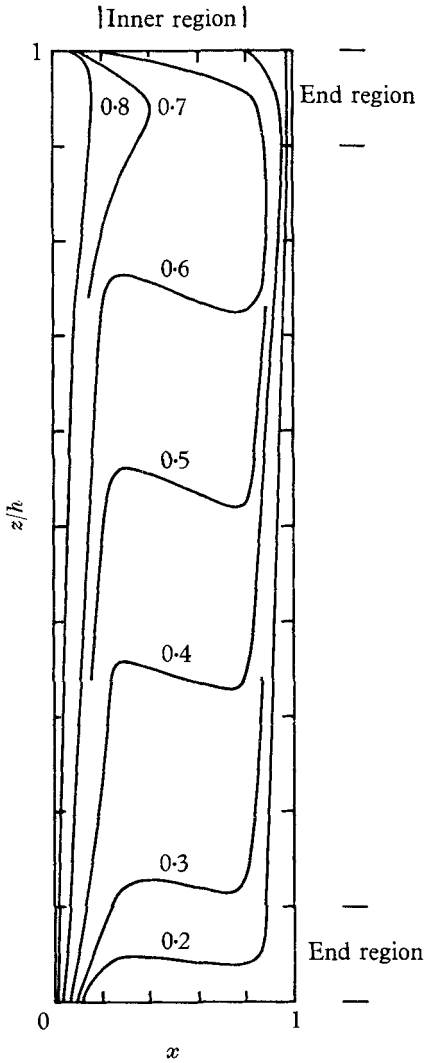

FIGURE 2. Temperature distribution: $h = 20$; $A = 4{\cdot}0 \times 10^5$ ($L = 3$ cm, $\Delta T = 16{\cdot}0$ °C paraffin). Note: vertical scale is $\frac{1}{5}$ horizontal scale. Lines drawn at constant values of θ.

is not sharply defined, but at small A it is of vertical extent about $2L$, at large A it is of extent $0{\cdot}1h$. On no occasion in the present investigation were secondary flows found to originate in the end regions, rather these always appeared to be regions of strong damping. Subsequent remarks therefore do not apply to the end regions.

4.2. *Temperature profile*

Temperature profiles at various values of z are shown in figure 3 by plotting $\Theta = \theta - \theta_m$ as a function of x, where $\theta = \theta_m$ when $x = \frac{1}{2}$. In the inner region $0{\cdot}2 < x < 0{\cdot}8$ all the points lie on the same curve, i.e. Θ is independent of z. Near the walls, however, Θ is a function of both x and z: θ_x decreasing as z increases along $x = 0$ and vice versa on $x = 1$.

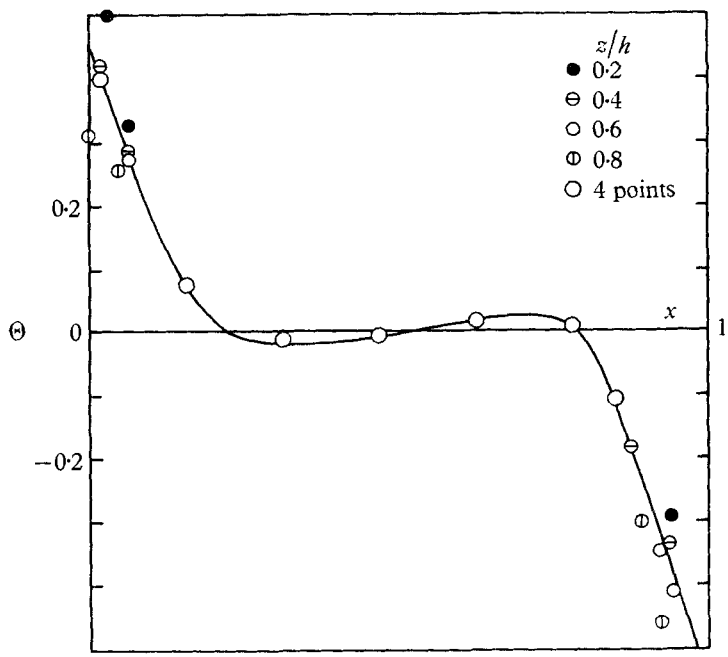

FIGURE 3. Temperature profile as a function of x, $\Theta = \theta - \theta_m$; $A = 4{\cdot}0 \times 10^5$, at four values of z/h.

4.3. *The vertical temperature gradient* β

Figure 4(*a*) shows values of θ_m as a function of z/h for *fixed* $h = 20$ at three values of A (i.e. 3 values of ΔT). Except near the ends, the temperature has a nearly uniform gradient $\beta \equiv d\theta_m/dz$. Note that the flow with $A = 6{\cdot}5 \times 10^5$ contains a secondary flow but the profile still has a pronounced linearity.

Figure 4(*b*) shows values of θ_m as a function of z/h for *fixed* $A = 1{\cdot}2 \times 10^6$ at four values of h (i.e. 4 values of H). Here also β is nearly constant. Note that quite small values of h are included, e.g. $h = 2{\cdot}5$.

4.4. *Magnitude of* β

Apparatus I was arranged with 3 thermocouples carefully mounted at $x = \frac{1}{2}$; $z/h = 0{\cdot}4$, $0{\cdot}5$, $0{\cdot}6$ and $y^* = \frac{1}{2}B$. The spacing L was set at 1·03 cm; silicone oil was used. This provided a direct measurement of β as a function of A (i.e. ΔT) without otherwise altering the apparatus. A direct-coupled amplifier was used to provide a precision of better than $\pm 0{\cdot}001$ °C. The temperature difference between pairs of thermocouples was measured directly. The results are shown in figure 5.

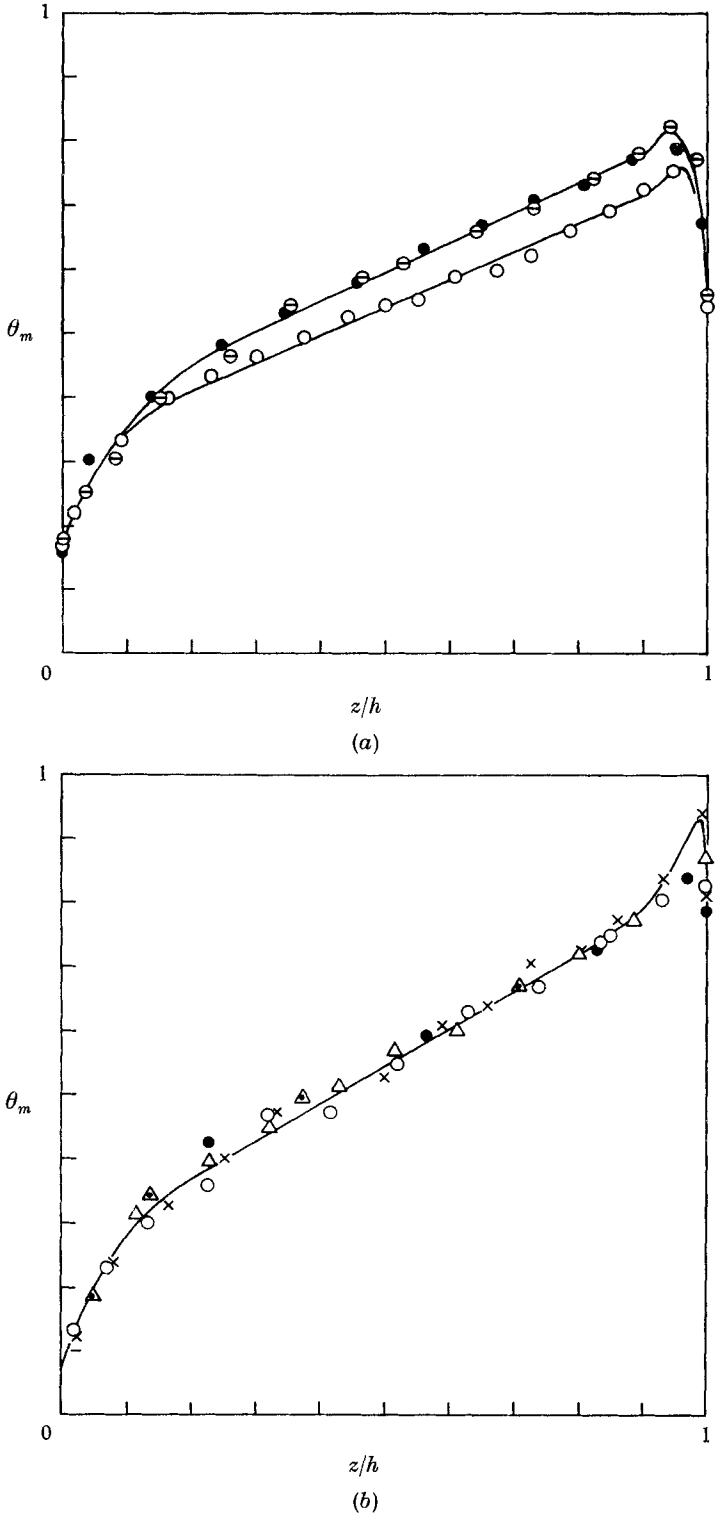

FIGURE 4. Centre-line temperature θ_m as a function of z/h: (*a*) Fixed $h = 20$ ($L = 2$ cm, apparatus I); A : $5{\cdot}6 \times 10^4$, $\ominus$; $1{\cdot}6 \times 10^5$, ●; $6{\cdot}5 \times 10^5$, ○. (*b*) Fixed $A = 1{\cdot}2 \times 10^6$ ($L = 4$ cm, apparatus II); h: 18·8, ○; 10·0, ×; 5·0, △; 2·5, ●.

Below $A = 10^4$, a non-zero value of β could not be found: between $A = 10^4 - 10^5$ a very rapid appearance of non-zero values of β occurs: beyond $A = 10^5$ up to at least $A = 10^8$, β achieves its asymptotic value; $\beta h \to 0{\cdot}50$ for paraffin, 0·55 for silicone 100 cS., while Eckert & Carlson's (1961) results for air give 0·60. Thus, βh is a weak function of Prandtl number. Note that β is approximately equivalent to the temperature gradient given by half the slot temperature drop established over the height of the slot.

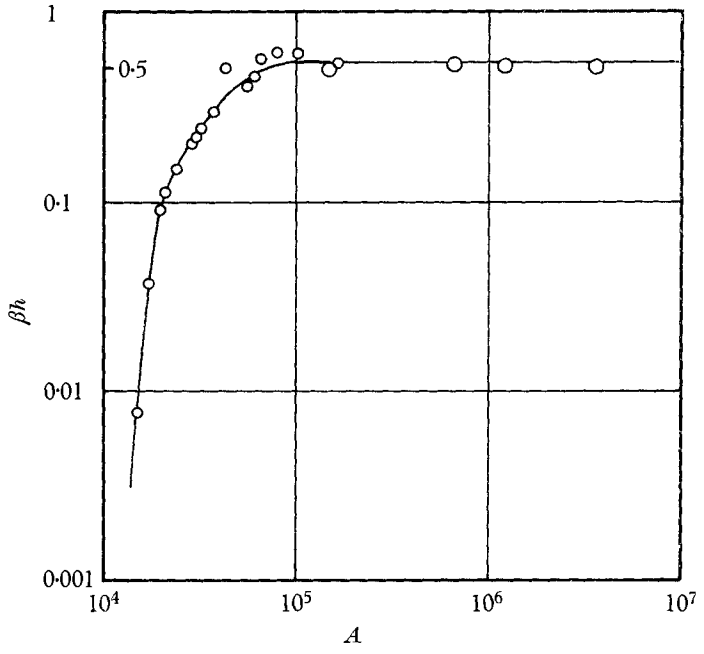

FIGURE 5. Centre-line vertical temperature gradient β. $L = 1{\cdot}03$ cm, apparatus I.

The value of β for given A was found to decrease a little at higher values of ΔT. Interpreting this as due to the variation of viscosity with temperature, all the paraffin data fit

$$\beta h = 0{\cdot}50[1 - 0{\cdot}04(\nu_0 - \nu_1)/\nu_1],$$

where ν_0, ν_1 are the kinematic viscosities evaluated at T_0 and $(T_0 + \Delta T)$, respectively.

4.5. *The velocity distribution*

Figure 6 shows experimental data for the velocity profile at $z = \frac{1}{2}h$ at four values of A. The various parameters are summarized in table 1. (The theoretical curves and f, m refer to the theory below. The values of f are fitted values.)

The profiles are all antisymmetric about $x = \frac{1}{2}$ as required by continuity and the symmetry of the boundary conditions, except for a tendency to higher velocities and smaller wall layer thickness in the flow near the hot wall produced by the variation of viscosity with temperature. Profile 6(*a*) has an inflexion point at $x = \frac{1}{2}$ and is very similar in form to that required as $A \to 0$. Profiles 6(*b*) and 6(*c*) have three inflexion points which become more widely separated as A

increases and the velocity profile becomes increasingly localized near the two walls. Profile 6(*d*) shows a small flow reversal in the region $0{\cdot}2 < x < 0{\cdot}8$.

Figure 7 shows the velocity profile at various values of z for fixed A, h ($H = 75{\cdot}7$ cm). The velocity is greatest near $z = \frac{1}{2}h$, but the profiles at $z^* = 30$, 40, 50 cm are indistinguishable.

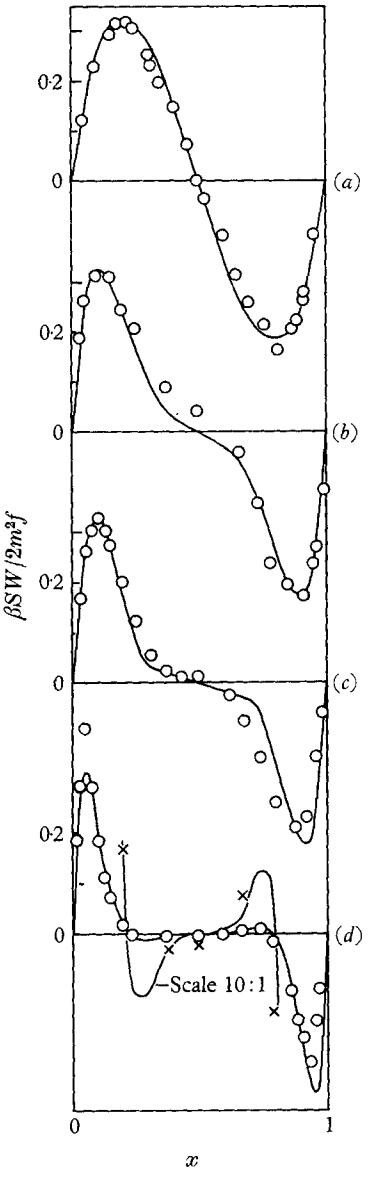

FIGURE 6. Velocity profiles at $z = \frac{1}{2}h$; apparatus I, paraffin, as specified in table 1; at various A: (*a*) $3{\cdot}08 \times 10^4$; (*b*) $2{\cdot}95 \times 10^5$; (*c*) $6{\cdot}56 \times 10^5$; (*d*) $3{\cdot}61 \times 10^6$. (The curves are calculated from (11*a*) with values of f given in table 1.)

4.6. *Experimental data on the inner flow as* $A \to \infty$

There is little experimental information for the inner flow at large Rayleigh numbers but the existing information strongly suggests that the inner region has zero vorticity and retains a finite, positive temperature gradient. This evidence is of necessity restricted to $A < 10^8$, for at about this Rayleigh number the motion is no longer steady.

Profile	L (cm)	H (cm)	ΔT (°C)	S	A	m	f
6(*a*)	2·00	38·8	5·40	50·6	$3{\cdot}08 \times 10^4$	3·75	0·25
6(*b*)	4·08	56·0	5·75	49·0	$2{\cdot}95 \times 10^5$	7·20	0·43
6(*c*)	4·08	56·5	11·6	46·7	$6{\cdot}56 \times 10^5$	8·70	0·48
6(*d*)	4·08	29·3	33·5	33·8	$3{\cdot}61 \times 10^6$	15·1	0·53

TABLE 1

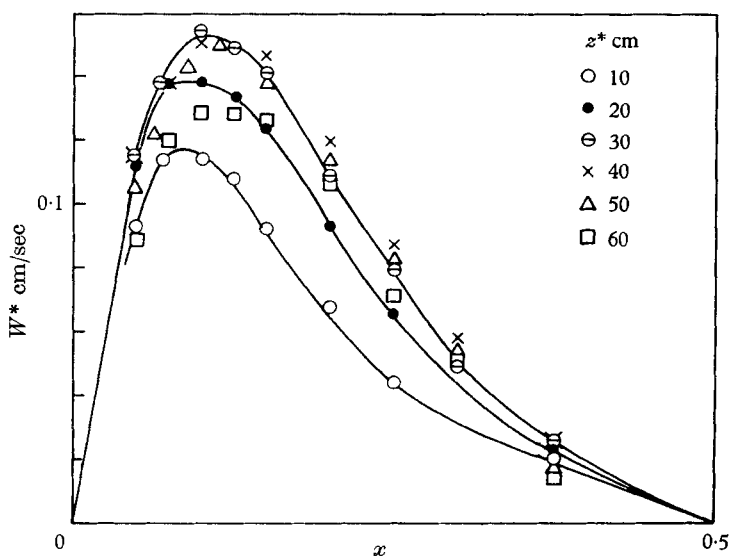

FIGURE 7. Velocity profiles for $L = 4{\cdot}08$ cm, $H = 75{\cdot}7$ cm, $A = 4{\cdot}0 \times 10^5$ at various values of z^*. Apparatus II.

Martini & Churchill (1960) used a gas-filled horizontal cylinder for which one side of the circumference was heated, the other cooled. They observed a ring of gas circulating in a boundary layer near the wall but with an apparently stagnant interior. Their observation generally agrees with the calculations of Weinbaum (1964).

Here a nearly square cavity ($h = 0{\cdot}92$) filled with silicone oil was observed at $A = 9{\cdot}4 \times 10^6$ ($L = 4{\cdot}8$ cm). The results are sketched in figure 8 drawn from a sequence of time photographs and confirmed by visual inspection. Note that here the upper and lower boundary conditions were identical—both surfaces being made with $\frac{1}{2}$ in. Perspex (previously the upper surface was free). Three distinct areas can be seen: (1) a wall region of strong clockwise circulation, in which

the streamlines closely follow the form of the wall; (2) a part of the interior adjacent to the vertical wall layers, also with clockwise circulation but in which the streamlines do not follow everywhere the form of the wall—these weak circulations are attached to the vertical layers and produce a weak return flow in the outer portion of the vertical layers; (3) the central part, or core, of the interior where no detectable flow could be observed, a velocity of 1 % of the

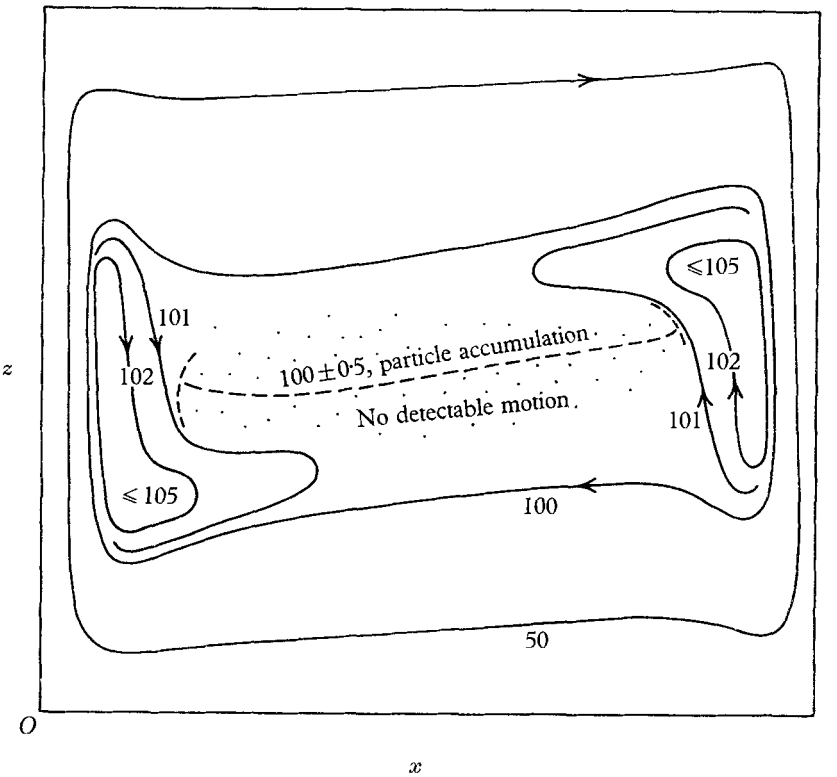

FIGURE 8. Streamlines of laminar flow in a nearly square cavity. $h = 0{\cdot}92$, $A = 9{\cdot}6 \times 10^6$. The stream function has been scaled to 100 units at the cavity centre. (VS 13: 26–32).

maximum found in the wall layer would have been easily detectable. However, the experiments did not find the motion in the core to be zero because, in the course of several runs, a characteristic distribution of the aluminium powder was found (admittedly this could have been established during the transient heating period), namely, a concentration of randomly oriented particles along a line near $z = \frac{1}{2}h$ as drawn in figure 8, suggesting a zone of both very small velocity and shear.

5. Experimental data for the secondary flows

5.1. *Onset of the secondary flow*

Figure 9 shows typical streamlines traced from photographs for flow in apparatus I with $L = 2{\cdot}00$ cm. In figure 9 (*a*), $A = 3{\cdot}0 \times 10^5$, the flow is unicellular; the streamlines circulate from one end of the slot to the other. In figure 9 (*b*), $A = 3{\cdot}6 \times 10^5$,

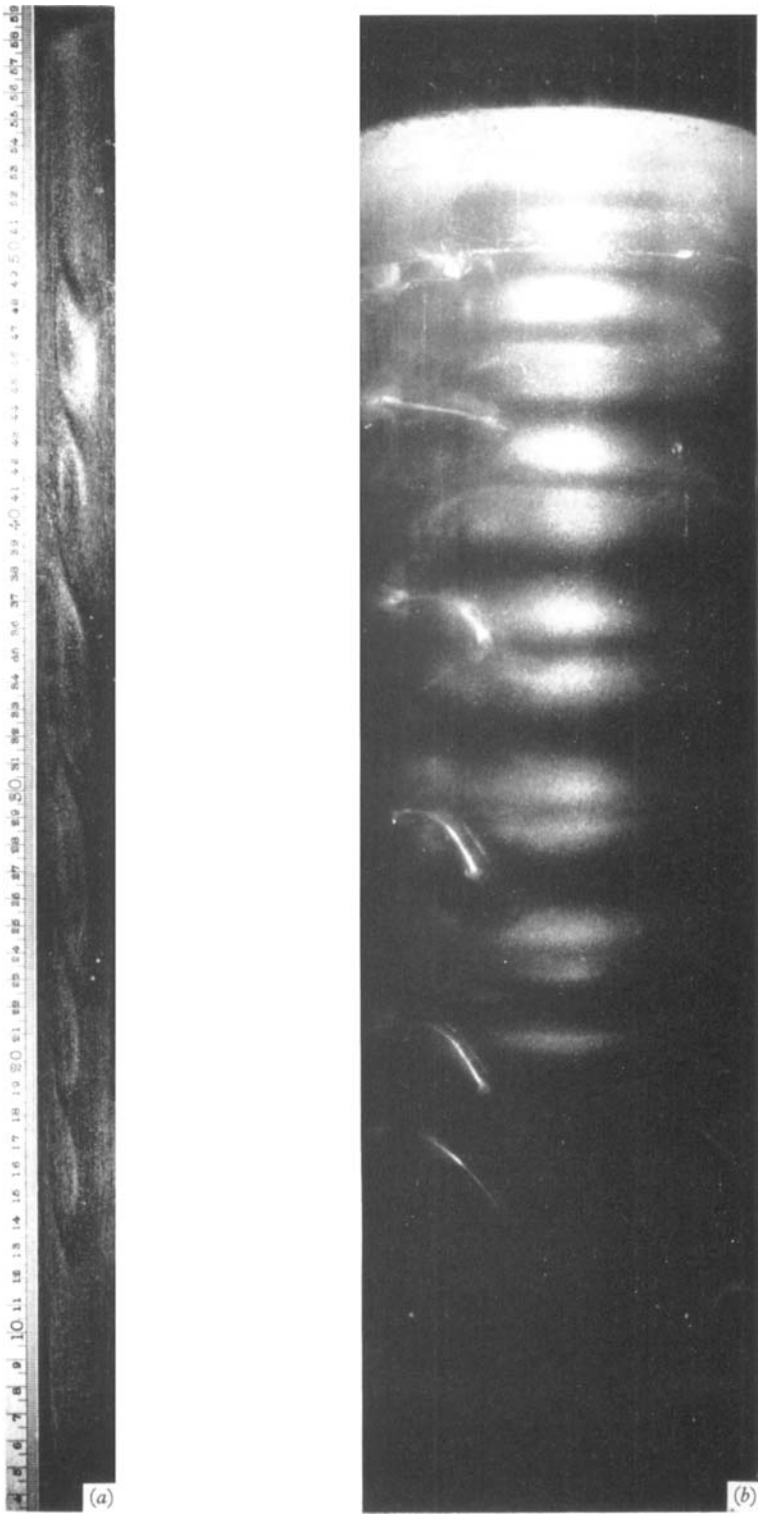

FIGURE 10. (*a*) Streak photograph of streamlines of the secondary flow; $A = 9 \times 10^5$, $L = 3$ cm, apparatus I. (VS 6: 19). (*b*) Photograph of the toroidal disturbances in the annulus of apparatus III; $A = 4{\cdot}8 \times 10^5$. The bright streaks on the left are thermocouple wires. (VP 3: 11.)

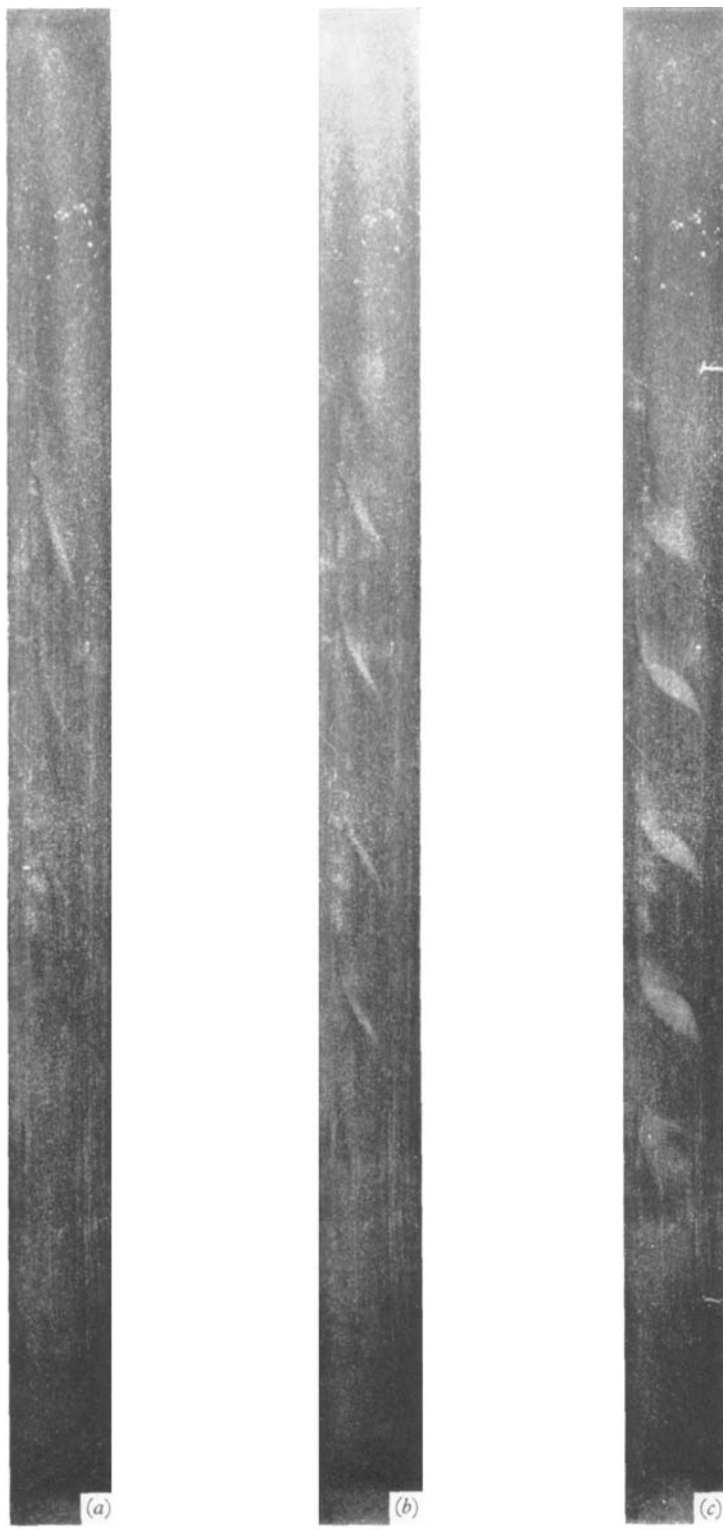

FIGURE 14. Streak photographs of streamlines of the secondary flow at various A, $L = 4{\cdot}08$ cm, showing the development of the tertiary flow: (*a*) $7{\cdot}1 \times 10^5$; (*b*) $9{\cdot}4 \times 10^5$; (*c*) $3{\cdot}3 \times 10^6$. (VS 9: 4, 5, 8.)

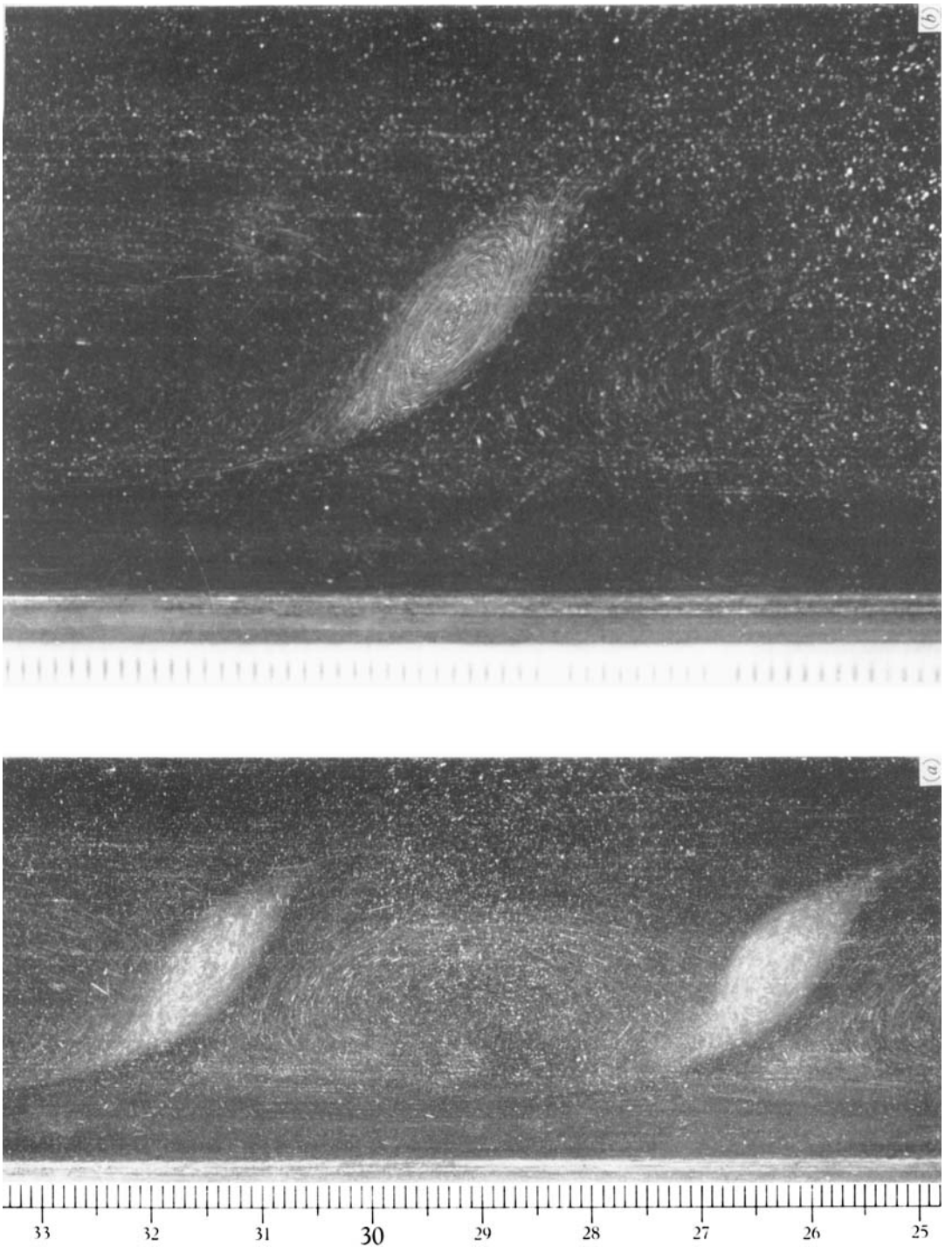

FIGURE 15. Detail streak photographs of the tertiary flow at $A = 3{\cdot}3 \times 10^6$, $L = 4{\cdot}08$ cm: (*a*) showing secondary and tertiary flow; (*b*) detail of tertiary flow-scale $1\frac{1}{2} \times$ (*a*). Compare figures 12 (2), 13, 14 (*c*). (VS 9: 10, 12. Exposure 5 sec.)

a second set of streamlines has appeared—one short cell and one which reaches to the upper-end region. These cells are very weak, and near the critical Rayleigh number are extremely difficult to detect, especially when the wavelength is large.

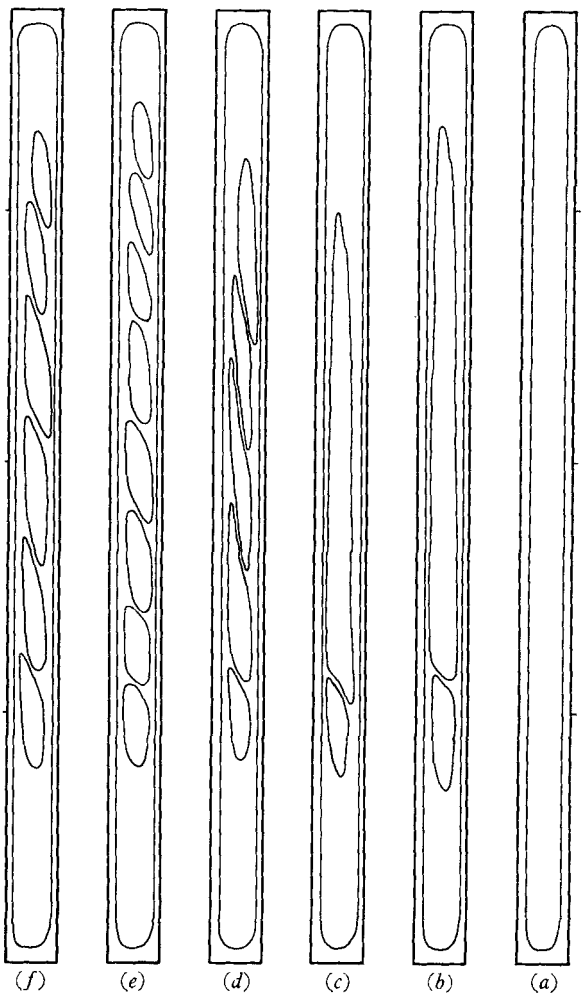

FIGURE 9. Sketch of streamlines of the secondary flow at various values of A: (*a*) $3{\cdot}0 \times 10^5$; (*b*) $3{\cdot}6 \times 10^5$; (*c*) $4{\cdot}0 \times 10^5$; (*d*) $4{\cdot}9 \times 10^5$; (*e*) $5{\cdot}8 \times 10^5$; (*f*) $6{\cdot}8 \times 10^5$. $L = 2$ cm, $H = 38$ cm, apparatus I (VS 2: 30–35).

As the Rayleigh number is increased the wavelength decreases, figure 9(*c*), and more cells can be fitted into the inner region, figures 9(*d*)–(*f*). In the experiments, critical temperature differences were 27 ± 2 °C, $6 \pm 0{\cdot}5$ °C, $4 \pm 0{\cdot}5$ °C for $L = 2, 3,$ 4 cm respectively, corresponding to a critical Rayleigh number of

$$A = 3 \times 10^5 \pm 30\ \%.$$

The large uncertainties are due to the difficulty of detecting the onset of the very weak secondary flow.

Figure 10(*a*) (plate 1) is a streak photograph for $A = 9 \times 10^5$. The gradual change of wavelength up the slot reflects the departure from uniformity of the primary flow. These departures are due to the large viscosity difference between the two walls.

Figure 10(*b*) (plate 1) is a photograph of the toroidal disturbances in the annular space of apparatus III. With this apparatus the cells grow first near $z = h$ and fill more and more of the lower slot as the heat flux is increased. This observation suggests that the appearance of the secondary flow is sensitive to the Rayleigh number since in this apparatus, with a uniform heat flux on the hot wall, the Rayleigh number increases vertically.

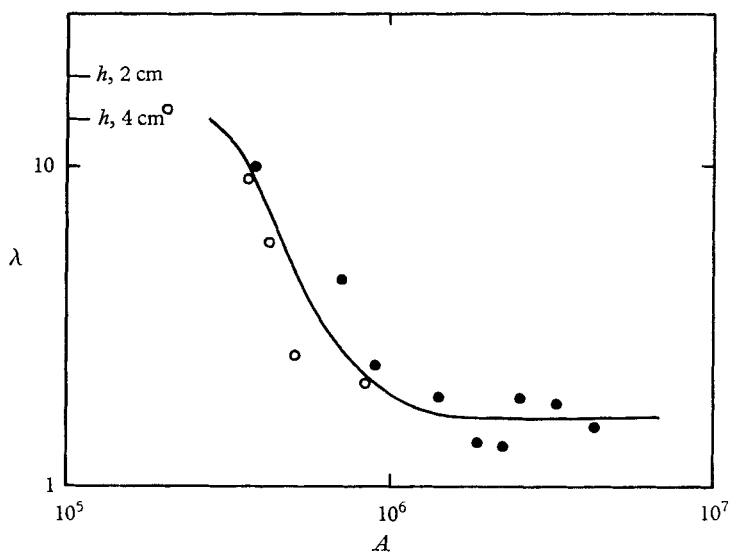

FIGURE 11. Vertical wavelength of the secondary flow as a function of A. ○, $L = 2{\cdot}00$ cm; ●, $L = 4{\cdot}00$ cm. Apparatus I.

These gross changes are summarized in figure 11 which relates the vertical wavelength λ measured near $z = \frac{1}{2}h$ to A. For all these experiments the initial secondary flow has a large wavelength of order H, so that the apparatus used was too short. There is a rapid decrease in λ as A increases.

5.2. *Non-linear effects*

As the disturbance amplitude increases, the disturbance begins to interact with the primary flow. Figure 12 shows θ_m for two values of A. For $A = 5{\cdot}3 \times 10^5$, which is near critical, the profile is closely linear away from the ends, except for a weak barely significant periodicity of wavelength $\lambda \doteqdot 8$. At $A = 3{\cdot}3 \times 10^6$ the oscillations are pronounced, with distinct and extensive portions where $d\theta_m/dz = 0$. Visual observation of the slot shows that the shear layers between each cell coincide with the regions of large temperature gradient $d\theta_m/dz$.

The interaction with the primary flow is strikingly shown in the temperature distribution of figure 13 for $L = 4{\cdot}08$ cm, $A = 3{\cdot}3 \times 10^6$. This pattern does not show the detail revealed in the streak photographs because of drift during

measurement and lack of sensitivity. While the $\theta = \beta z + \Theta(x)$ variation is still dominant in the inner region, the isotherms are both steepened and given a periodic variation of spacing. The local temperature variation due to the disturbances is $\pm 0{\cdot}015\,\Delta T$ in figure 13. Colder fluid is carried from near the cold wall across the slot and up the hot wall where it is heated and again carried across the slot to the cold wall.

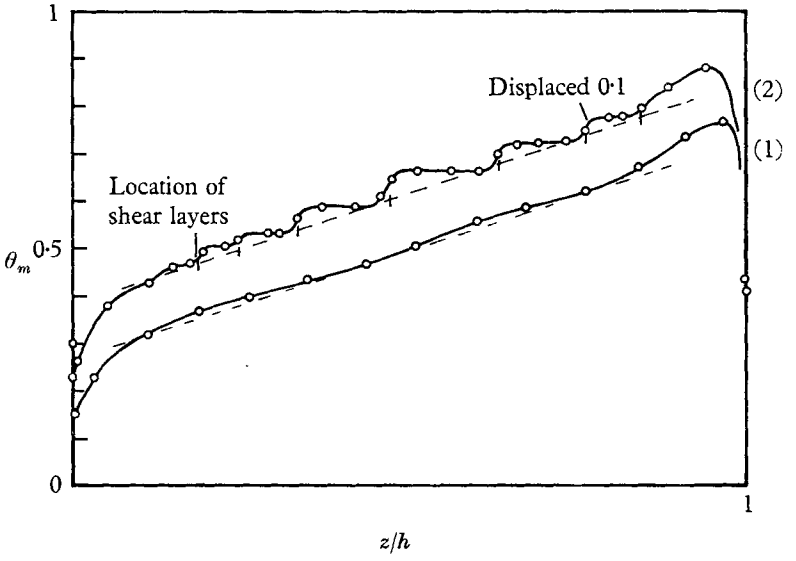

FIGURE 12. Centre-line temperature θ_m when the secondary flow is present, $L = 4{\cdot}08$ cm; (1) $A = 5{\cdot}3 \times 10^5$; (2) $A = 3{\cdot}3 \times 10^6$. The position of the shear layers between cells is indicated.

5.3. *The tertiary flow*

The most intriguing feature of this study occurs near $A = 10^6$ and is shown in the photographs of figure 14 (plate 2) obtained with apparatus II. Again at lower Rayleigh numbers the primary flow is unicellular; the first appearance of the secondary flow is similar to that shown in figures 9 and 10, but as the Rayleigh number is increased a pronounced and rapid change is observed in the weak shear layers between successive cells of the secondary flow. The shear layers become thicker, the bright lozenge-shaped patterns indicate that the aluminium particles are trapped and suggest that a new flow has appeared. Close inspection confirms this. Figure 15(*a*) (plate 3) shows a close-up of a 'cats-eye' of the secondary flow, together with tertiary flows in the shear layers. (The photograph is somewhat obscured by motions occurring close to the nearside glass side.) In figure 15(*b*) the camera has been carefully focused on the tertiary flow and reveals a circulation with closed streamlines. While the primary and secondary flows have the same sense of circulation (clockwise in the figures) the tertiary flow is in the opposite sense (anticlockwise in the figures). The sense of circulation is not shown by the photographs but is easily observed by eye.

Detailed measurements of the tertiary flow are difficult. The velocity distribution can be measured with acceptable accuracy but the temperature variation

produced by the secondary flow is only of order $\pm 0{\cdot}02\,\Delta T$. In figure 15 (*b*) the tertiary cell is at 55° to the vertical, of thickness 6 mm, length 16 mm, has a temperature difference of 2·0 °C and a velocity change of 1·24 mm/sec across it.

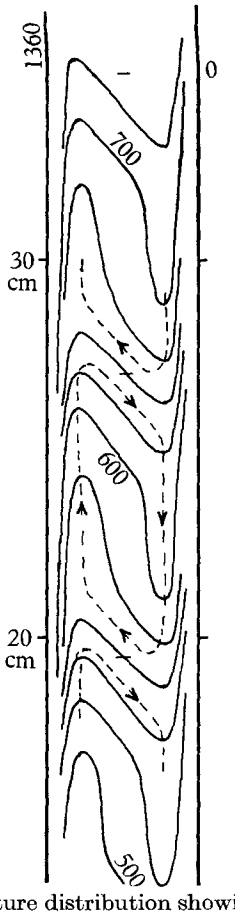

FIGURE 13. Detail of the temperature distribution showing the interaction of the primary and secondary temperature field. Isotherms are in units of 1/40 °C. $A = 3{\cdot}3 \times 10^6$; $L = 4{\cdot}08$ cm.

6. Discussion of the primary flow

6.1. *Formulation of the problem*

The aim of the discussion below is a tentative attempt to elucidate the mechanisms involved in the primary flow. We are interested in the flow for all possible values of A, h and S. But clearly there will be substantial differences in the details of the flows for $h \gg 1$, where the buoyancy field and the velocity field are parallel over the greater portion of the slot, and $h \ll 1$, where the two fields are generally perpendicular. Here our concern is with $h \gg 1$. In addition, the experiments reported here were performed with $\sigma \doteqdot 10^3$. Our principal concern therefore is to discuss the flow as a function of A for given $h \gg 1$ and $S \gg 1$.

The field equations relating the variables density, temperature, velocity and pressure are those of conservation of mass, momentum, energy and the equation

of state. These can be made dimensionless by choosing units of length, temperature, pressure, and velocity, as in (2). For $h \gg 1$ the equations can be simplified by means of a boundary-layer-type approximation, $\partial^2/\partial x^2 \gg \partial^2/\partial z^2$. This implies that the lateral rate of diffusion of momentum and heat is much more rapid than the vertical rate. Consequently, the x-momentum equation is of lower order than that of the z-momentum equation. Therefore, the pressure $P = P(z)$. Thus in dimensionless variables, with the simplification $p = P + \rho g z$, and the Boussinesq approximation,

$$U_x + W_z = 0, \tag{3a}$$

$$UW_x + WW_z = -Bp_z(z) + A\theta + SW_{xx}, \tag{3b}$$

$$U\theta_x + W\theta_z = \theta_{xx}/S, \tag{3c}$$

where $B = gL^3/\kappa\nu$. These equations must satisfy $U = W = 0$ on $x = 0, 1$; $\theta = 1, 0$ on $x = 0, 1$ and suitable conditions on $z = 0, h$.

In general, the analysis will ignore the end regions, so that, unless otherwise stated, the calculations refer only to some region near $z = \frac{1}{2}h$.

6.2. *The interior region*

We notice that the entire flow field is symmetrical about the central point $x = \frac{1}{2}, z = \frac{1}{2}h$. In particular, continuity requires $U = 0$ on $z = \frac{1}{2}h$ so that in some interior region near $x = \frac{1}{2}, z = \frac{1}{2}h$, where $U \doteqdot 0$, inertial effects will be negligible.

In some region near $x = \frac{1}{2}, z = \frac{1}{2}h$ consider the consequences of writing $U = 0$. From (3)

$$W_z = 0, \tag{4a}$$

$$A\theta = Bp_z(z) - SW_{xx}, \tag{4b}$$

and

$$SW\theta_z = \theta_{xx}. \tag{4c}$$

This is a flow which is independent of z, in which buoyancy forces are balanced by viscous forces and the vertical pressure gradient, inertial forces being identically zero. Heat is transported horizontally solely by thermal conduction and vertically solely by advection.

Hence $W \equiv W(x)$, and (4b) shows θ as the sum of a function of x and a function of z. Substituting for θ in (4c)

$$BSWp_{zz} = -SW_{xxxx}. \tag{5}$$

Since $W \equiv W(x)$ and $p \equiv p(z)$, this is only possible if

$$p_{zz} = \text{const.} \tag{6}$$

Hence, from (4b)

$$\beta \equiv \theta_z = \text{const.} \tag{7}$$

Note that the equations (4) could have been derived directly from the complete equations with $U = 0$. An extra term θ_{zz} would then be found in (4c) and hence a term Bp_{zzz} in (5). But this does not alter the argument, since in both cases the proposed solution is only possible if $p_{zz} = \text{const.}$ It should therefore be remembered that the form of the interior solution relies only on the assumption $U = 0$ and not on the boundary-layer-type approximation.

6.3. *The existence of a non-zero vertical temperature gradient*

The form of the interior solution can now be found provided β is known. There are two obvious possibilities $\beta = 0$ or $\beta > 0$.

Consider $\beta = 0$. From (4*b*) $p_z = $ const. and from (4*c*) $\theta_x = $ const. It is now seen that a solution valid for *all* x can be obtained to satisfy the boundary conditions $\theta = 1, 0$; $W = 0$ on $x = 0, 1$, that is

$$\theta = 1 - x, \tag{8a}$$

and from (4*b*)
$$12SW = Ax(1-x)(1-2x). \tag{8b}$$

Now as shown by Batchelor (1954), using an expansion in powers of A, this is the solution to order A, distant from the ends. (The result itself can be obtained directly from the equations of motion by writing $\theta_z, W_z = 0$.) That is to say, for given h, there will be values of A sufficiently small for (8) to be valid. Otherwise, however, for values of A such that $\theta \neq (1-x)$ we expect $\beta \neq 0$.

6.4. *The form of the solution in the interior region for* $A \gg 1$

For $\beta > 0$, substituting for p_{zz} from (4*b*) in (5), we obtain

$$(D^4 + 4m^4)\, W = 0, \tag{9}$$

where
$$4m^4 = \beta A, \tag{10}$$

and $D = d/dx$. This has solutions of the form $\exp mx(\pm 1 \pm i)$. If m is sufficiently large, a suitable solution for W is,

$$W = (2m^2 f/\beta S)\,(e^{-mx} \sin mx - e^{-m\bar{x}} \sin m\bar{x}), \tag{11a}$$

writing $\bar{x} = 1 - x$. Whence from (4*b*)

$$\theta = \theta_m(z) + f(e^{-mx} \cos mx - e^{-m\bar{x}} \cos m\bar{x}), \tag{11b}$$

where
$$\theta_m = Bp_z/A = \tfrac{1}{2} + \beta(z - \tfrac{1}{2}h), \tag{11c}$$

and f is (at the moment) an arbitrary constant. Note that the forms of W and θ are antisymmetric about $x = \frac{1}{2}$ as required by the centro-symmetry of the entire flow. It must be emphasized that (11) is only valid if m is sufficiently large for there to be a region of no vertical motion and uniform temperature gradient between the wall layers and that even then it is only valid in the parts of the wall layers furthest from the wall.

The solution (11) strictly applies only near $x = \frac{1}{2}$, $z = \frac{1}{2}h$, but we notice, if $e^{-m} \ll 1$, that on $x = 0, 1$ $W \doteqdot 0$ and $\theta = 1, 0$ if

$$f = 0{\cdot}5. \tag{11d}$$

The vertical temperature gradient β remains as an unknown constant.

The form of the solution (11) agrees fairly well with the temperature data of figure 3 and the velocity data of figure 6. The experimental values of f, given in table 1, are moderately close to 0·5. The value $f = 0{\cdot}25$ at $A = 3{\cdot}08 \times 10^4$ is, however, rather low and suggests that this particular flow is not in the limiting state for which β is independent of A. The progressive change in the velocity

profile with increasing m, in particular the flow reversal revealed in figure 6(d), is nicely predicted. The region over which (11) is satisfactory, within the experimental accuracy, is roughly the central half of the slot.

6.5. *A discussion of the flow as a whole*

The flow can be considered as an interaction between two thermal boundary layers, one on the hot wall, the other on the cold wall. Consider an infinite stationary body of fluid at temperature $\theta_m = \frac{1}{2}$, in which are placed two vertical plates, one heated to a temperature $\frac{1}{2}$ above that of the ambient fluid, the other cooled by an equal amount. If the plates are widely separated the flow near one plate can be expected to be independent of the other plate. Let us concentrate attention for the moment on the flow near the hot plate. Then, as seen in Squire's calculations (Goldstein 1938), which uses the method of von Kármán and Pohlhausen, the velocity in the thermal boundary layer, which grows near the wall, is nearly vertical except for the small entrainment velocity $U \equiv U(z)$. In Squire's calculation, therefore, the ambient fluid, distant from the plate, is at a uniform temperature but has a horizontal velocity which is a function of height. Similar remarks apply to the cold plate. But the $U(z)$ required for an isolated plate cannot simultaneously satisfy the requirements of both plates.

The role of the vertical temperature gradient in this process is seen in equation (3b). Near $z = 0$ the buoyancy forces exceed the viscous forces and accelerate the fluid, but owing to the vertical temperature gradient the buoyancy force diminishes, till at $z = \frac{1}{2}h$ it is balanced by the viscous forces. The fluid is decelerated beyond $z = \frac{1}{2}h$. It should be noted that outside the wall layers there will be an entrainment flow $U(z)$. Near $z = \frac{1}{2}h$, $U \doteqdot 0$ as required by continuity and the symmetry of the boundary conditions, but in the regions of growth of the wall layers $U \neq 0$. Thus $U < 0$ for $z < \frac{1}{2}h$, and $U > 0$ for $z > \frac{1}{2}h$ corresponding to entrainment of fluid into the growing layers but out of the layers beyond their point of maximum growth. These features are clearly demonstrated by Eckert & Carlson's (1961) measurements.

In §§ 6.3 and 6.5 we have solutions for the two cases $\beta = 0$ and $\beta = \text{const}$. These can be interpreted in the above terms as follows. The case $\beta = 0$ corresponds to the two boundary layers each completely filling the slot. Heat is transferred across the slot by thermal conduction only, the consequent motion corresponding to a balance between buoyancy and viscous forces. Heat and momentum are transferred solely by diffusion. The case $\beta = \text{const.}$ corresponds to a complete separation of the two layers, producing an interior of almost no motion and zero horizontal temperature gradient. In this case no heat is transferred between the two layers. Hence, on integrating (4c) from $x = 0$ to $x = \frac{1}{2}$,

$$\beta \sim -\theta_x(0) \Big/ \int_0^{\frac{1}{2}} SW\,dx. \tag{12}$$

Since $W_z \doteqdot 0$ near $z = \frac{1}{2}h$, this equation merely states that for a constant mass flow, $\int_0^{\frac{1}{2}} SW\,dx$, and heat input, $-\theta_x(0)$, there will be a constant vertical temperature gradient θ_z. This situation does not arise for an isolated vertical plate

because the fluid is accelerating and can transport the accumulated heat, diffused into the layer from the wall, as increased advection and by heating entrained ambient fluid.

Experimentally, we have found that βh is a constant, nearly independent of A and S for A and S sufficiently large. It is not surprising that βh is independent of S, since it is well known that the gross features of free convective flows are nearly independent of S for S large. The following crude argument suggests a possible form for $\beta = \beta(S, A, h)$. From (4c)

$$\beta \sim \theta_{xx}/SW. \tag{13}$$

For the purpose of estimating the right-hand side of (13) assume that the layers grow in a manner similar to that on an isolated plate. Then in Squire's solution for $S \gg 1$ it is seen that $\theta_{xx} \sim 1/\delta^2 \sim (A/h)^{\frac{1}{2}}$, where δ is the boundary-layer thickness, and $SW \sim (Ah)^{\frac{1}{2}}$. Hence

$$\beta \sim 1/h. \tag{14}$$

The agreement of this with the experiments suggests that, at least in part, the layers grow like those on an isolated plate. The measurements of heat-transfer coefficient given by Eckert & Carlson (1961) confirm this suggestion. More importantly this suggests that β arises from the interaction of the boundary layers, viz. by inhibiting entrainment, rather than arising from effects in the end regions with mere conduction of heat from the hot upper to the cold lower end producing the gradient.

An estimate of the Rayleigh number at which β becomes finite can be obtained by noticing that for $\theta = 1 - x$,

$$W \propto x(1-x)(1-2x),$$

which has a maximum at

$$x_W = (1 - 1/\sqrt{3}) = 0{\cdot}211.$$

The solution $W \propto e^{-mx} \sin mx$ has a maximum near $x_i = \pi/4m$. Clearly, we must have $x_i < x_W$, hence $m \geqslant 1{\cdot}22\pi$. If we take $\beta = 0{\cdot}5/h$, since $4m^4 = \beta A$,

$$A \geqslant 1770h. \tag{15}$$

It also follows that the solution obtained above cannot be expected to be valid unless $A > 1770h$. This limit for the change from conductive to convective domination is in reasonable agreement with experiment (q.v. figure 5).

7. A remark on the primary flow as $A \to \infty$

The solution of § 6 suggests that, as $A \to \infty$, there will be a uniform vertical temperature gradient and no motion almost everywhere in the slot. Undoubtedly there will be boundary layers on the walls but, since these have a thickness proportional to $A^{-\frac{1}{4}}$, they will be infinitesimally thin as $A \to \infty$.

This deduction differs from the suggestion of Pillow (1952) and Batchelor (1954) that the flow should have constant non-zero vorticity and uniform temperature almost everywhere. In the limiting case proposed by Batchelor and Pillow the non-linear terms are important everywhere in the slot, whereas the present formulation is based on the assertion that in the inner region these

terms are negligible. In the present experiments this is certainly the case, because the non-linear terms are seen to be dominant only in the wall layers, so that since the boundary layers are infinitesimally thin as $A \to \infty$, the non-linear terms would be zero everywhere except for sheets on the walls.

It is worth remarking here on a physically erroneous idea I have frequently encountered while talking about this problem. The motion in the boundary layers appears to provide a torque on the inner fluid thereby giving vorticity to the interior. This is not so for finite Prandtl number. The motion in the boundary layer does generate a torque, but as seen in (4*b*) this is balanced by the torque due to the horizontal gradient of buoyancy forces. As seen in § 6, the vorticity in the fluid falls rapidly to zero as the outer portion of the boundary layer is approached.

8. Discussion of the secondary and tertiary flows

Above $A \sim 10^5$ a steady secondary flow appears in the interior region with streamlines resembling a 'cats-eye' pattern. Such a pattern can be produced by superimposing a periodic secondary motion upon a shear flow. However, a curious feature of the secondary flow is the strong tilting of the shear layers between the cells (e.g. see figures 10 (*a*), 14 and 15, plates 1, 2, 3). This feature can be reproduced if the periodic secondary motion has lines of constant phase inclined to the horizontal, so that the temperature and stream function of the secondary motion θ, ψ have, e.g., the form

$$(\theta, \psi) = \{u(x), v(x)\} \sin\{rx + sz + \epsilon(x)\}. \tag{16}$$

In the experiments u, v become zero at $x, \bar{x} = d < \frac{1}{2}$. Consider the following example. Let the primary stream function be $\frac{1}{2}\zeta(x+\frac{1}{2})^2$, corresponding to a uniform shear. A suitable form for $v(x)$ is $v(x) = C\{d^2 - (x+\frac{1}{2})^2\}^2$, since then $\psi, \psi_x = 0$ on $x = \frac{1}{2} \pm d$. Thus consider the total stream function

$$\psi_* = \psi / \tfrac{1}{2}\zeta d^2 = x'^2 + \xi(1 - x'^2)^2 \sin(rx + sz), \tag{17}$$

where $x' = (x+\frac{1}{2})/d$ and $\xi = 2d^2C/\zeta$ is a measure of the secondary-flow amplitude relative to that of the primary flow. Figure 16 shows the streamlines for $s/r = 0{\cdot}4$, a value for the data of figures 10 (*a*), 14 and 15, $r = \pi/d$ when $\xi = 0{\cdot}2, 1$. When ξ is sufficiently small, as in figure 16 (*a*), the circulation is everywhere of the same sign, equal to that of the primary flow. The secondary flow has unit cells of vertical wavelength equal to that of the perturbation but displaced vertically a quarter wavelength. When ξ is sufficiently large, as in figure 16 (*b*), the flow is as before except for regions of reversal of circulation near the position of the shear layer between the original cells. Here are our so-called tertiary flows.

The condition for the appearance of the tertiary flows is simply that $\psi_{*x} = 0$ at points $0 < |x'| < 1$. For our present example this requires $\xi > \frac{1}{2}$. In the experiments ξ increases with Rayleigh number both because the perturbation amplitude increases and because ζ decreases as the flow becomes increasingly localized near the walls.

In so far as the description (16) of the motion is valid, namely, that the cells of opposite circulation are due to a strengthening of the secondary flow relative to the primary flow, the possibility that the tertiary flows arise from an instability of the secondary flow is discounted.

I was greatly helped in preparing this manuscript by numerous comments from Dr B. R. Morton, Dr A. E. Gill and Mr P. J. Bryant. I should like to acknowledge the assistance of Mr W. G. Garner who built most of the apparatus. This work has been supported by the British Admiralty. The manuscript was written while I was supported by a National Science Foundation Grant GP-2414 and an Office of Naval Research Contract Nonr-2216.

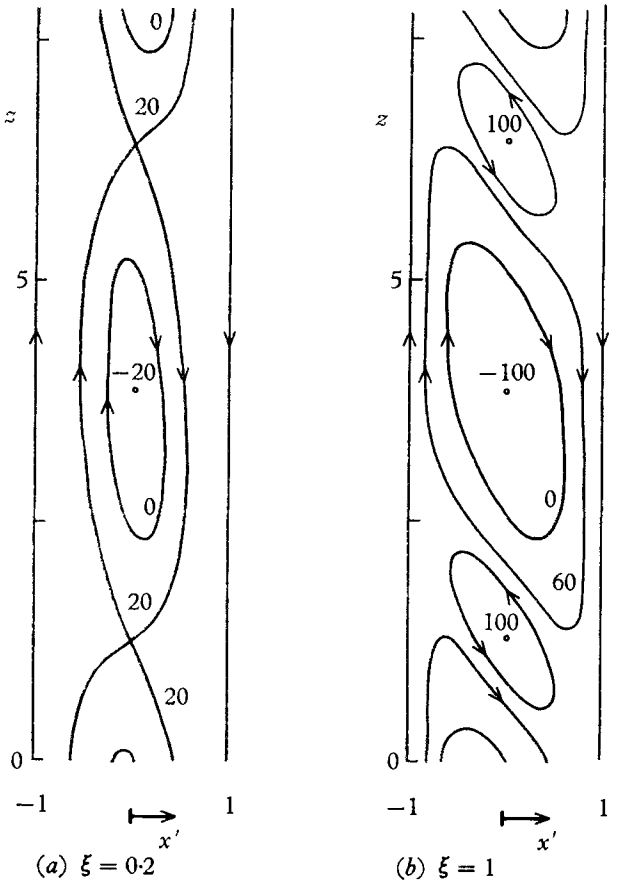

FIGURE 16. Sketch of streamlines given by (17) for two values of the relative perturbation amplitude: (*a*) $\xi = 0{\cdot}2$, showing the secondary flow; (*b*) $\xi = 1$, showing the tertiary flow.

REFERENCES

BATCHELOR, G. K. 1954 *Quart. Appl. Math.* **12**, 209.

ECKERT, E. R. G. & CARLSON, W. O. 1961 *Int. J. Heat & Mass Transfer*, **2**, 106.

GOLDSTEIN, S. 1938 Ed. *Modern Developments in Fluid Dynamics*. Oxford University Press.

MARTINI, W. R. & CHURCHILL, S. W. 1960 *A.I.Ch.E.J.* **6**, 251.

MORDCHELLES-REGNIER, G. & KAPLAN, C. 1963 *Proc. Int. Heat & Mass Transfer Conf.* 94.

PILLOW, A. F. 1952 *Austr. Aero. Res. Rep.* no. A79.

SCHLICHTING, H. 1960 *Boundary Layer Theory*. London: Pergamon Press.

WEINBAUM, S. 1964 *J. Fluid Mech.* **18**, 409.